Appl Phys A
DOI 10.1007/s00339-012-6757-1

Applied Physics A
Materials Science & Processing

INVITED PAPER

Tunable Fano resonances in silver–silica–silver multilayer nanoshells

Jin Fa Ho · Boris Luk'yanchuk · Jing Bo Zhang

Received: 7 July 2011 / Accepted: 8 December 2011

Abstract We study the plasmonic properties of silver–silica–silver multilayer nanoshells using finite-difference time-domain methods. Silver is a weakly dissipating metal and is able to support higher order resonances compared to strongly dissipating metals like gold. We show that Fano resonances occur even in symmetric cases. Symmetry breaking via the introduction of core offset further enhances these Fano resonance peaks and leads to the appearance of higher order resonances. The optical properties of the multilayer nanoshells are explained using the plasmon hybridization theory and the results are compared to similar multilayer nanoshells with gold core and outer shell.

1 Introduction

Fano resonance is a widely studied phenomenon in various quantum systems, such as nanowires, tunnel junctions and quantum dots [1–3], with many potential applications for narrowband optical filters, polarization selectors, modulators, switches and sensors. There have been a few attempts [4, 5] to produce Fano resonance in classical optics, but structures to achieve this are necessarily complicated because it is difficult to achieve narrow surface plasmon resonance peaks in classical optics. In weakly dissipating plasmonic materials, Fano resonance can arise due to the interference between a broad Mie resonance and a narrow surface plasmon resonance [6]. Fano resonances can be observed in various plasmonic nanostructures [7–10] due to the overlapping of broad dipole and narrow quadrupole resonances in plasmonic materials. Interference of these resonances can be observed as an N-shaped profile in differential scattering spectra. Localized plasmons excited by the incident light are equivalent to the quasi-discrete levels in the Fano approach, while the radiative decay of the excitation plays the same role as tunneling from quasi-discrete levels [11]. Thus, the local maximum and minimum in scattering spectra correspond to constructive and destructive interference between different eigenmodes, respectively. A symmetric Lorentzian profile is always observed in the vicinity of the dipole resonance, while an asymmetric Fano resonance profile may be observed in the vicinity of the quadrupole resonance. The quadrupole resonance exhibits extremely high sensitivity to the frequency of the incident light, where small variations can change forward scattering to backward scattering [12–14]. This offers potential applications in the development of highly sensitive biochemical sensors [15].

In essence, Fano resonances are analogous to coupled harmonic oscillator systems [16]. The spectral positions of localized plasmon resonances depend sensitively on the shape and geometry of the underlying subwavelength metallic structures [17], making them ideal systems to realize classical oscillators at the nanoscale. The resonance can be easily tuned from the visible to the near-infrared region by changes in the geometry of the nanostructures. Fano resonance is commonly achieved in nanostructures with two or more plasmonic particles via symmetry breaking [18–21]. Symmetry breaking introduces coupling between broad bright dipolar modes and higher order narrow dark modes as multipolar resonances in the metallic nanostructures are no longer orthogonal [22]. This leads to a hybridization of the plasmonic modes, which can be used to tune the wavelength of the Fano resonance [23]. Core–shell

J.F. Ho · B. Luk'yanchuk (✉) · J.B. Zhang
Data Storage Institute, Agency for Science, Technology and Research, Engineering Drive 1, Off Kent Ridge Crescent, NUS, 117608 Singapore, Singapore
e-mail: Boris_L@dsi.a-star.edu.sg
Fax: +65-651-60900

Published online: 19 January 2012

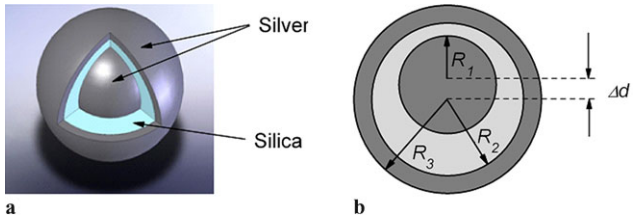

Fig. 1 (**a**) 3D illustration of silver–silica–silver MNS. (**b**) Dimensions of an R_1–R_2–R_3 silver–silica–silver multilayer nanoshell with core offset Δd

nanoshells (CNSs) and multilayer nanoshells (MNSs) are commonly employed in the study of plasmon hybridization theory [24]. Optical properties of MNSs and CNSs can be explained by bonding and antibonding type combinations of fundamental plasmon resonances of the constituent plasmonic particles. Studies of gold–silica–gold MNSs [25, 26] show that adding a gold core to a silica–gold CNS splits the low-energy plasmon resonance into a high-energy antibonding mode and a low-energy bonding mode that can be tuned from the visible to the infrared region by varying the silica layer thickness. A study of varying the offset of the core [24] also shows a red shift of the dipolar bonding mode and a blue shift of the antibonding mode.

In this paper, we propose the use of silver, a weakly dissipating metal, in metal–dielectric–metal MNSs. With weakly dissipative metals, higher order resonances which cannot be seen with a highly dissipative metal like gold can now be seen in the visible range of the electromagnetic spectrum [27, 28]. We compare the results to recent studies of gold–silica–gold MNSs [25, 26]. The extinction spectra and field properties of the silver–silica–silver MNSs are simulated using Lumerical FDTD Solutions v 6.5.10. The FDTD (finite-difference time-domain) calculations were performed with a multicoefficient fit to experimental permittivity data for silver [29]. The SiO_2 dielectric layer was calculated using a dielectric constant of $\varepsilon = 2.14$. The computational model for the MNSs is shown in Fig. 1, and is characterized by four parameters, R_1, R_2 and R_3, corresponding to the radius of each layer, and Δd corresponding to the core offset. The background index is modeled after air with a refractive index of 1.

2 Results and discussion

We start by investigating the properties of concentric silver–silica–silver MNSs with $\Delta d = 0$. Figure 2 shows the far-field forward and backward scattering intensity profiles of a 50–66–75 nm concentric MNS. The scattering behavior can be explained using an exact Mie solution [11]. The dipole mode at 1038 nm plays a dominant role in background scattering with high intensity relative to the contributions of the

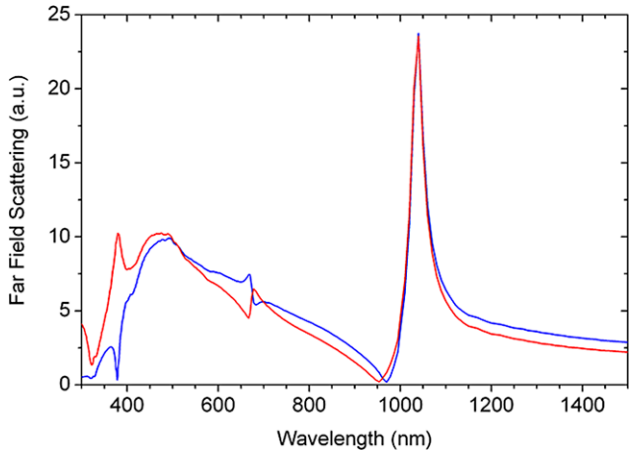

Fig. 2 Far-field backward scattering (*blue*) and forward scattering (*red*) for 50–66–75 nm MNS. The symmetric dipole resonance can be seen in the vicinity of 1038 nm. Asymmetric quadrupole resonances are seen around 390 and 670 nm; the forward and backward scattering profiles in these vicinities are typical of Fano resonances

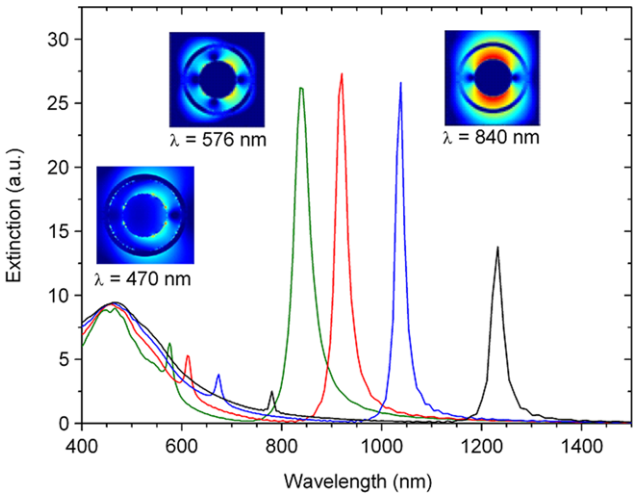

Fig. 3 Extinction spectra for concentric MNS with $R_2 = 66$ nm and $R_3 = 75$ nm as a function of R_1 for: $R_1 = 40$ nm (*green*), 45 nm (*red*), 50 nm (*blue*) and 55 nm (*black*). *Insets*: electric field intensity plots for 40–66–75 nm MNS (*green curve*). The narrow and broad dipole resonances can be seen, as well as the quadrupole Fano resonance

other modes because silver is a weakly dissipating material. For the quadrupole modes at 390 and 670 nm, destructive interference for the forward and backward scattering lie on different sides of the resonance peak. This is typical for Fano resonances, and there is a high angular distribution sensitivity of the scattered light. Small variations of incident light frequency in this vicinity change the scattering from preferentially forward to preferentially backward. The effects of varying the core size are shown in Fig. 3. The tunability of the Fano resonance from the visible yellow to the near-infrared range is demonstrated. Decreasing the silver-core radius leads to a red shift in both the narrow dipole and the quadrupole peaks, while the broad dipole peak at 470 nm

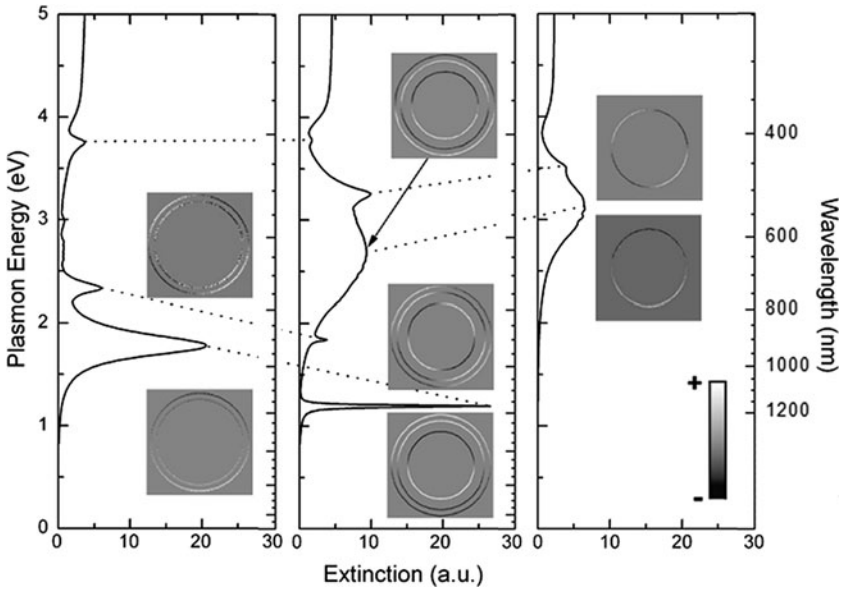

Fig. 4 Plasmon hybridization diagrams for 50–66–75 nm MNS in vacuum. Extinction spectra are for silica-core silver-shell CNS (*left-hand panel*), MNS (*center panel*) and silver core (*right-hand panel*). The *insets* show the surface charge distributions at the corresponding resonance energies

remains relatively unchanged. To understand this, we will use plasmon hybridization to analyze the spectral response of the MNSs.

The optical properties of the silver–silica–silver MNSs can be explained as a hybrid between a silver core and a silica-core silver-shell CNS. Qualitatively, the spectral response of the multilayer MNSs can be modeled by a system of coupled oscillators [26]. Figure 4 shows the plasmon hybridization diagram for the concentric 50–66–75 nm MNSs. The hybridization between the silver core's dipole mode and the silver shell's dipole mode results in a broad, superradiant high-energy mode and a narrow, subradiant low-energy mode in the MNSs. The low-energy MNS bonding modes below 2.0 eV have narrow radiative widths. It is clearly seen from the charge distributions that the symmetric bonding modes of the silica-core silver-shell CNS are oppositely aligned with the silver-core modes, resulting in the subradiant nature of the MNS modes. With a larger core radius, there is greater coupling between the plasmon modes of the core and the shell, resulting in the red shift of the subradiant dipole and quadrupole modes as they are repelled by interactions with higher order modes. The superradiant antibonding dipole mode at 2.7 eV remains unchanged when the core radius is varied, even though a red shift is expected corresponding to the red shift of the dipole energy level of a silver nanoshell as its radius is increased from 40 to 55 nm. This effect is exactly balanced by the blue shifting caused by interactions with the lower energy subradiant quadrupole mode, which increases with core radius size.

The bonding-type hybridization between the oppositely aligned shell quadrupole mode and core quadrupole mode gives rise to a subradiant quadrupole mode in the combined MNS structure. This subradiant quadrupole mode couples to the superradiant dipole mode, resulting in a Fano resonance at 1.83 eV. While plasmon hybridization between multipolar resonances of different orders in the shell and the core are forbidden due to orthogonality in concentric nanostructures, the 50–66–75 nm MNS is sufficiently large and lies beyond the electrostatic limit where orthogonality no longer holds [30]. It is worthwhile to compare this with results on similar concentric gold–silica–gold MNSs [26] with radii parameters of 35–50–75 nm, where Fano resonance arises due to the coupling between the subradiant dipole mode and the superradiant dipole mode. For silver–silica–silver MNSs, the Fano resonance arises from coupling between the subradiant quadrupole mode and the superradiant dipole mode. The subradiant dipole mode does not overlap the superradiant dipole mode spectrally and has a much higher amplitude compared to the gold–silica–gold MNSs.

3 Effects of symmetry breaking

With non-concentric geometries, it becomes easier for multipolar resonances to interact and produce Fano resonances. Figure 5 shows the effects of increasing core offset for a 50–66–75 nm MNS. The major effects are a red shift of resonance peaks, the appearance of higher order Fano resonances and a suppression of the dipole mode. Red shifting of the resonance peaks is caused by greater interactions between core and shell modes due to increased offset. Coupling between higher order modes that appear with increased offset and lower order modes repels the lower order modes to higher wavelengths. At the largest offset ($\Delta d = 15$ nm) calculated, dipole to hexadecapole field distributions are observed. By varying the offset of the core, both the intensity and the spectral position of Fano resonance peaks can be controlled. These effects are very similar

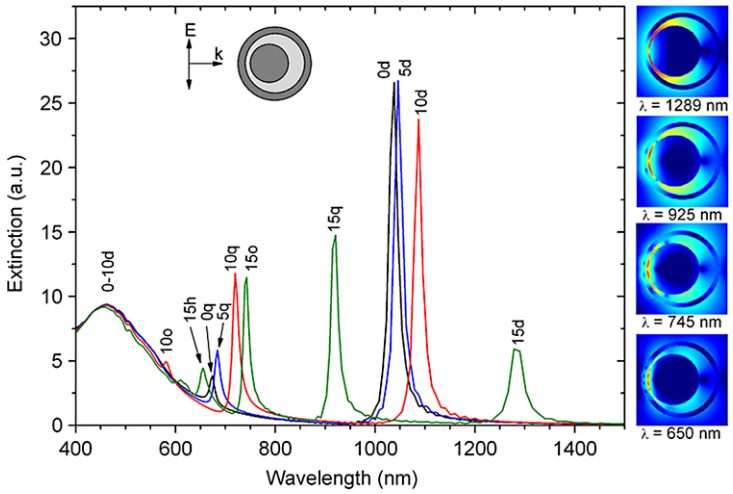

Fig. 5 Extinction spectra for 50–66–75 nm MNS as a function of core offset: $\Delta d = 0$ nm (*black*), 5 nm (*blue*), 10 nm (*red*) and 15 nm (*green*). Dipole (d), quadrupole (q), octupole (o) and hexadecapole (h) peaks are labeled accordingly. E-field polarization is perpendicular to the axis of symmetry. Insets: electric field intensity plots for $\Delta d = 15$ nm (*green curve*)

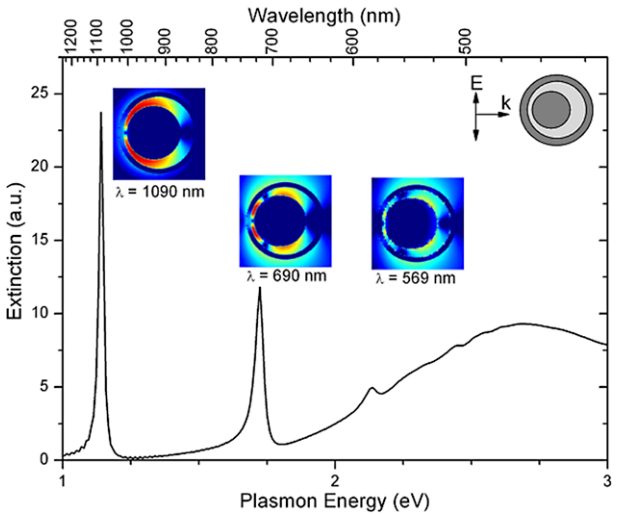

Fig. 6 Extinction spectrum and field distributions for 50–66–75 nm MNS with $\Delta d = 10$ nm. The hybridized natures of the quadrupole and octupole modes are seen in the field distributions

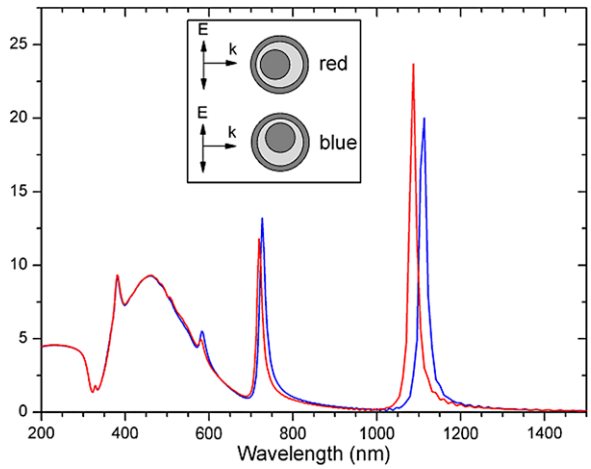

Fig. 7 Extinction spectra for 50–66–75 nm MNS with different particle orientations. *Red curve*: incident electric field is polarized perpendicular to axis of symmetry. *Blue curve*: incident electric field is polarized parallel to axis of symmetry

to those observed in 35–50–75 nm gold–silica–gold MNSs [26], where red shifting and higher order peaks appear with greater offset. However, the silver–silica–silver MNSs allow for greater enhancement of higher order peaks and can sustain multiple pronounced Fano resonances in the visible frequencies.

Resonance modes are more distinguishable with a 50–66–75 nm MNS with $\Delta d = 10$ nm, shown in Fig. 6. The subradiant dipole mode at 1090 nm remains uncoupled to the superradiant dipole mode, while the quadrupole and octupole modes at 690 and 569 nm couple to the superradiant dipole mode to produce Fano resonances. The hybridized natures of the quadrupole and octupole modes are seen in the field distribution profiles. While the silica layer shows quadrupole and octupole distributions, the shell layer shows a dipole distribution. The asymmetric MNS displays an almost isotropic response as shown in Fig. 7. Different orientations of the MNS produce very similar spectra. However, it is important to note that for orientations with greater asymmetry for a given electric field polarization, effects similar to offsetting the core are observed. Electric field polarization parallel to the axis of symmetry gives rise to systems with greater asymmetry and there is a red shift and suppression of the dipole mode, along with enhancement of the quadrupole and octupole modes.

4 Conclusion

In conclusion, we have shown that silver–silica–silver MNSs are ideal for producing Fano resonances in the visible wavelengths. Tuning of Fano resonance locations can be achieved via the variation of core size or the introduction of a core offset. The amount of offset can also be used to enhance and control the intensity of Fano resonance peaks

while suppressing the subradiant dipole resonance. Thus, weakly dissipating materials such as silver have advantages over strongly dissipating materials such as gold for producing interference of broad and narrow resonances, which results in pronounced Fano resonances.

Acknowledgements The authors would like to acknowledge the financial support of the grant JCOAG03-FG04-2009 from the Joint Council of Agency for Science, Technology and Research (A*STAR) of Singapore, and the grant TSRP-1021520018 from the Science and Engineering Research Council (SERC) of A*STAR of Singapore.

References

1. H.G. Luo, T. Xiang, X.Q. Wang, Z.B. Su, L. Yu, Phys. Rev. Lett. **92**, 256602 (2004)
2. A.C. Johnson, C.M. Marcus, M.P. Hanson, A.C. Gossard, Phys. Rev. Lett. **93**, 106803 (2004)
3. K. Kobayashi, H. Aikawa, A. Sano, S. Katsumoto, Y. Iye, Phys. Rev. B **70**, 035319 (2004)
4. U. Fano, J. Opt. Soc. Am. **31**, 213 (1941)
5. H.T. Lee, A.W. Poon, Opt. Lett. **29**, 5 (2004)
6. U. Fano, Phys. Rev. **124**, 1866 (1961)
7. N. Liu, L. Langguth, T. Weiss, J. Kästel, M. Fleischhauer, T. Pfau, H. Geissen, Nat. Mater. **8**, 758 (2009)
8. C. Genet, M.P. van Exter, J.P. Woerdman, Opt. Commun. **225**, 331 (2003)
9. A. Christ, S.G. Tikhodeev, N.A. Gippius, J. Kuhl, H. Giessen, Phys. Rev. Lett. **91**, 183901 (2003)
10. M. Rahmani, B. Lukiyanchuk, B. Ng, A.K.G. Tavakkoli, Y.F. Liew, M.H. Hong, Opt. Express **19**, 4949 (2011)
11. M.I. Tribelsky, S. Flach, A.E. Miroshnichenko, A.V. Gorbach, Y.S. Kivshar, Phys. Rev. Lett. **100**, 043903 (2008)
12. B.S. Luk'yanchuk, M.I. Tribelsky, V. Ternovsky, Z.B. Wang, M.H. Hong, L.P. Shi, T.C. Chong, J. Opt. A, Pure Appl. Opt. **9**, S294 (2007)
13. M. Rahmani, B. Lukiyanchuk, T.T.V. Nguyen, T. Tahmasebi, Y. Lin, T.Y.F. Liew, M.H. Hong, Opt. Mater. Express **1**, 1409 (2011)
14. B.S. Luk'yanchuk, M.I. Tribelsky, Z.B. Wang, Y. Zhou, M.H. Hong, L.P. Shi, T.C. Chong, Appl. Phys. A **89**, 259 (2007)
15. L. Niu, J.B. Zhang, Y.H. Fu, S. Kulkarni, B. Luk'yanchuk, Opt. Express **19**, 22974 (2011)
16. Y.S. Joe, A.M. Satanin, C.S. Kim, Phys. Scr. **74**, 259 (2006)
17. S.A. Maier, Nat. Mater. **8**, 699 (2009)
18. F. Hao, Y. Sonnefraud, P.V. Dorpe, S.A. Maier, N.J. Halas, P. Nordlander, Nano Lett. **8**, 3983 (2008)
19. N. Verellen, Y. Sonnefraud, H. Sobhani, F. Hao, V.V. Moschchalkov, P.V. Dorpe, P. Nordlander, S.A. Maier, Nano Lett. **9**, 1663 (2009)
20. F. Hao, P. Nordlander, Y. Sonnefraud, P.V. Dorpe, S.A. Maier, ACS Nano **3**, 643 (2009)
21. V.A. Fedotov, M. Rose, S.L. Prosvirnin, N. Papasimakis, N.I. Zheludev, Phys. Rev. Lett. **99**, 147401 (2007)
22. P. Nordlander, ACS Nano **3**, 488 (2009)
23. E. Prodan, C. Radloff, N.J. Halas, P. Nordlander, Science **302**, 419 (2003)
24. Y. Hu, S.J. Noelck, R.A. Drezek, ACS Nano **3**, 1521 (2010)
25. Y. Hu, R.C. Fleming, R.A. Drezek, Opt. Express **16**, 19579 (2008)
26. S. Mukherjee, H. Sobhani, J.B. Lassiter, R. Bardhan, P. Nordlander, N.J. Halas, Nano Lett. **10**, 2694 (2010)
27. M.I. Tribelsky, B.S. Luk'yanchuk, Phys. Rev. Lett. **97**, 263902 (2006)
28. B. Luk'yanchuk, N.I. Zheludev, S.A. Maier, N.J. Halas, P. Nordlander, H. Giessen, T.C. Chong, Nat. Mater. **97**, 707 (2010)
29. P.B. Johnson, R.W. Christy, Phys. Rev. B **6**, 4370 (1972)
30. F. Tam, A.L. Chen, J. Kundu, H. Wang, N.J. Halas, J. Chem. Phys. **127**, 204703 (2007)